Inorg. Chem. **2006**, *45*, 2068–2074

New Synthesis Route to and Physical Properties of Lanthanum Monoiodide†

Mikhail Ryazanov, Lorenz Kienle, Arndt Simon,* and HansjUrgen Mattausch

Max-Planck Institut für Festkörperforschung, Heisenbergstrasse 1, D-70569 Stuttgart, Germany

Received October 24, 2005

A fast procedure to produce LaI by reduction of LaI_2 or LaI_3 in a Na melt under argon at 550 °C is given. The structural studies performed by means of powder X-ray diffraction as well as transmission electron microscopy are consistent with previous single-crystal results. Measurements of the electrical resistance on polycrystalline samples reveal metallic behavior for LaI in the range 10–300 K. Upon cooling, a small maximum in the resistivity has been observed at 67 K. This anomaly disappears upon heating a sample, however, yielding a hysteresis in $\rho(T)$ above 70 K. From the Pauli susceptibility, an electron density of states at the Fermi level of about 0.3 eV^{-1}·formula $unit^{-1}$ has been estimated, as compared with a value of 1.0 eV^{-1}·formula $unit^{-1}$ derived from ab initio LMTO band structure calculations.

Introduction

The chemistry of the rare-earth elements has been restricted for a long time to ionic trivalent lanthanide compounds with the exception of some divalent (Eu^{2+}, Yb^{2+}) and tetravalent (Ce^{4+}) compounds, whose existence has been associated with the special stability of $4f^0$, $4f^7$, and $4f^{14}$ electronic configurations. During the past few decades there has been great progress in the preparation of binary Ln_aX_b and ternary halides of the rare-earth metals in low oxidation states.[1−10] In general, these are reduced compounds which either adopt saltlike structures (e.g., LnI_2; Ln = Sm, Eu[6]) or contain metal−metal bonded structural units, often stabilized by interstitial atoms (e.g., GdI_2,[7] Gd_2Cl_3, Gd_2X_2C, $GdXH_x$; X = Cl, Br, and I).[4] The latter metal-rich phases are of particular interest because they have been found to exhibit many interesting chemical and physical properties. Superconducting $La_2X_2C_2$ phases[8,9] and ferromagnetic GdI_2, which shows a very large negative magnetoresistance (∼65%) at room temperature,[10] would be good examples.

Another remarkable example is the lanthanum monoiodide, LaI, a binary lanthanide halide with the lowest ratio X/Ln = 1 found so far. This compound with virtually monovalent La atoms is indeed the only known stable solid-state monohalide of the rare-earth elements, first synthesized and studied in 1995 by Corbett and Martin.[5] It crystallizes in a NiAs-type structure with a remarkably large value of the *c*/*a* ratio (*c*/*a* = 2.47). According to structural analysis and extended Hückel band structure calculations, two electrons are delocalized in the conduction band, so that LaI is expected to exhibit metallic properties.

A convenient and frequently used route to synthesize reduced lanthanide halides is via reduction of trihalides (LnX_3) with the respective Ln metal according to $n\ LnX_3 + (3 - n)Ln \rightarrow 3LnX_n$. These synproportionation reactions are profitable thermodynamically in terms of achieving equilibrium, and there is no need for subsequent isolation or separation of desired products.[11] Nonetheless, often high

† Dedicated to Professor John D. Corbett on the occasion of his 80th birthday.

* To whom correspondence should be addressed. E-mail: a.simon@fkf.mpg.de.

(1) Mee, J. E.; Corbett, J. D. *Inorg. Chem.* **1965**, *4*, 88−93.
(2) Corbett, J. D. *Rev. Chim. Miner.* **1973**, *10*, 239−257.
(3) Meyer, G. *Chem. Rev.* **1988**, *88*, 93−107.
(4) Simon, A.; Mattausch, Hj.; Miller, G. J.; Bauhofer, W.; Kremer, R. K. In *Handbook on the Physics and Chemistry of Rare Earths*; Gschneidner, K. A., Jr., Eyring, L., Eds.; North-Holland Publisher: Amsterdam, 1991; Vol. 15, p 191.
(5) Martin, J. D.; Corbett, J. D. *Angew. Chem.* **1995**, *107*, 234−236; *Angew. Chem. Int. Ed. Engl.* **1995**, *34*, 233−235.
(6) Bärnighausen, H. *Rev. Chim. Miner.* **1973**, *10*, 77−92.
(7) Kasten, A.; Müller, P. H.; Schienle, M. *Solid State Commun.* **1984**, *51*, 919−921. Bärnighausen, H. *Proceedings Hauptversammlung der Gesellschaft Deutscher Chemiker*; Wiley-VCH: München, 1997; p 74.
(8) Simon, A.; Mattausch, Hj.; Eger, R.; Kremer, R. K. *Angew. Chem.* **1991**, *103*, 1209−1210. *Angew. Chem., Int. Ed. Engl.* **1995**, *30*, 1188−1189.
(9) Simon, A.; Yoshiasa, A.; Bäcker, M.; Henn, R. W.; Felser, C.; Kremer, R. K.; Mattausch, Hj. *Z. Anorg. Allg. Chem.* **1996**, *622*, 123−137.
(10) Felser, C.; Ahn, K.; Kremer, R. K.; Sheshadri, R.; Simon, A. *J. Solid State Chem.* **1999**, *147*, 19−26.
(11) Corbett, J. D. In *Synthesis of Lanthanide and Actinide Compounds*; Meyer, G., Morss, L. R., Eds.; Kluwer Academic Publishers: Dordrecht, 1991.

10.1021/ic051834r CCC: $33.50
Published on Web 01/25/2006

temperatures and longer reaction times are required to complete these solid-state reactions. This makes the synproportionation route less efficient for a quantitative synthesis of such reduced halide phases that are only stable in a temperature range where neither a significant vapor pressure of the trihalide nor a molten state are present. This is the case for LaI, where heating of appropriate mixtures of LaI_3/La at elevated temperatures for several weeks resulted only in small yields of the reduced halide.[5]

Alternatively, some reduced halides of the rare-earth elements can successfully be synthesized by direct reactions of the elements[12−14] or by "metallothermic" reductions of lanthanide(III) halides with alkali metals.[15−18] The latter method has a long history. Already in 1937, Klemm and Bommer used potassium as a reducing agent in reactions with $LnCl_3$ to produce metal powders of almost all the rare-earth elements.[16] Later, Meyer and co-workers succeeded in preparing a series of binary and ternary halides of the divalent lanthanides using the same synthetic approach.[15,17] According to recent studies,[18] metal-rich sesquihalides Ln_2Br_3 (Ln = Gd, Tb) can also be synthesized by sodium reduction of the Ln(III) bromides. The main advantage of the metallothermic reductions compared to synproportionation reactions is that the former are quite fast due to the presence of a melt at fairly low temperatures. As a drawback, the reduced halides prepared via this route need to be separated from other reaction coproducts. In addition, the starting lanthanide(III) halides as well as its reduced products can react with alkali metal halides produced during the reaction to form stable ternary phases, thus prohibiting a ready synthesis of binary reduced halides.

Here, we report a new high-yield synthesis for LaI together with measurements of some physical properties. The results of first principles electronic structure calculations for LaI are also presented.

Experimental Section

Syntheses. All compounds were handled under purified Ar either in a glovebox (H_2O < 0.2 ppm; O_2 < 0.8 ppm) or by employing standard Schlenk techniques. La metal pieces (99.99%; Johnson Matthey, Germany) and iodine powder (99.8%; Merck) were utilized as starting materials. Sodium (99%; Cl < 0.01%, K < 0.05%) was purchased from Merck and refined before use by filtration. LaI_3 was prepared by a direct reaction of the elements in an evacuated sealed silica tube at 900 °C[19] and further purified by two subsequent sublimations at 930 °C in high vacuum (10^{-4} Torr). Lanthanum diiodide was obtained by heating a 2:1 mixture of LaI_3 and La filings at 800 °C for 3 days. This mixture was ground, pelletized, and then heated in an arc-welded Ta ampule filled with argon, the container of choice for subsequent reactions. To prevent oxidation of the containers, these were further sealed in evacuated silica jackets.

Lanthanum monoiodide was synthesized by reduction of LaI_2 or LaI_3 with Na in a 1:1 (or 1:2.2) proportion, respectively. The reaction mixtures with desired amounts of the starting materials (a total weight of ∼500 mg) were loaded into Ta containers within a glovebox and then heated at 500−550 °C for a few (3−7) days to 2 weeks.

To extract co-formed NaI from the reaction products, these were treated with several fractions of anhydrous diethylene glycol dimethyl ether (diglyme: 99.5%, H_2O < 100 ppm; Aldrich). The isolated product was dried in a dynamic vacuum at room temperature until the pressure was reduced to the initial values (∼10^{-3} Torr).

Differential Thermal Analysis (DTA). DTA curves were recorded on a self-constructed computer-controlled setup equipped with an Eurotherm 818S temperatures/process controller and a Hewlett-Packard 3457A multimeter. γ-Al_2O_3 was used as a reference substance. A mixture of LaI_2 and Na with the ratio 1:1 (∼100 mg) sealed within a 5 mm diameter tantalum tube, was heated under argon to 1200 K with a rate of 5 K/min, and then was cooled to approximately 400 K with the same rate. Such a heating/cooling cycle was repeated two times.

Electron Microscopy. HRTEM (high-resolution transmission electron microscopy) and SAED (selected area electron diffraction) was performed with a Philips CM30ST electron microscope (300 kV, LaB_6 cathode, C_S = 1.15 mm). All manipulations needed for the preparation and transfer of the sample were carried out under dry argon using a self-constructed device.[20] A perforated carbon/copper net served as a support for the crystallites. Simulations of the HRTEM images (multislice formalism) and of SAED patterns (kinematical approximation) were calculated with the EMS program package[21] (spread of defocus, 70 Å; illumination semiangle, 1.2 mrad). All images were recorded with a Multiscan charge-coupled device camera (software Digital Micrograph 3.6.1 (Gatan)) and were filtered after Fourier transformation. EDX (energy-dispersive X-ray) spectroscopy analysis was performed in the nanoprobe and in the scanning mode of CM30ST with a Si/Li-EDX detector (Noran, Vantage System).

Powder X-ray Analysis. The microcrystalline samples of LaI were sealed in glass capillaries (diameter, 0.2 mm) filled with Ar. X-ray diffraction patterns were recorded in Debye−Scherrer geometry on a Stoe Stadi P diffractometer (Mo Kα radiation, λ = 0.7093 Å, germanium monochromator). Lattice dimensions and atomic parameters were refined by Rietveld analysis using the FullProf program.[22] The pseudo-Voigt function was used for simulation of the peak shapes. All reflections were corrected for asymmetry (2θ < 40°) and preferred orientation effects using the March−Dollase function.[23] The final Rietveld refinement pattern is plotted in Figure 1.

Crystallographic data and refinement parameters for LaI are as follows: hexagonal, space group $P6_3/mmc$ (No. 194), a = 3.9292(1) Å, c = 9.712(1) Å, La in 2a (0,0,0) with B_{iso} = 1.03(3) Å^2, I in 2c (1/3,2/3,1/4) with B_{iso} = 1.24(4) Å^2, V = 129.85(2) Å^3, Z = 2,

(12) Bochkarev, M. N.; Fagin, A. A. *Chem.−Eur. J.* **1999**, *5*, 2990−2992.
(13) Khoroshenkov, G. V.; Petrovskaya, T. V.; Fedushkin, I. L.; Bochkarev, M. N. *Z. Anorg. Allg. Chem.* **2002**, *628*, 699−702.
(14) Evans, W. J.; Allen, N. T.; Workman, P. S.; Meyer, J. C. *Inorg. Chem.* **2003**, *42*, 3097−3099.
(15) Meyer, G.; Schleid, T. In *Synthesis of Lanthanide and Actinide Compounds*; Meyer, G., Morss, L. R., Eds.; Kluwer Academic Publishers: Dordrecht, 1991.
(16) Klemm, W.; Bommer, H. *Z. Anorg. Allg. Chem.* **1937**, *231*, 138−171.
(17) Meyer, G.; Schleid, Th. *Inorg. Chem.* **1987**, *26*, 217−218.
(18) Beck, U. Ph.D. Thesis, University of Stuttgart, Stuttgart, Germany, 1995.
(19) Brauer, G. *Handbuch der Präparativen Anorganischen Chemie*; Ferdinand Enke Verlag: Stuttgart, 1978; Vol. 2.
(20) Jeitschko, P.; Simon, A.; Ramlau, R.; Mattausch, Hj. *Eur. Microsc. Anal.* **1997**, *46*, 21.
(21) Stadelmann, P. A. *Ultramicroscopy* **1987**, *21*, 131−145.
(22) Rodriguez-Carvajal, J. *FullProf 2k*, Version 2.50; LLB CEA-CNRS: Gif sur Yvette, France, 2003.
(23) Dollase, W. A. *J. Appl. Crystallogr.* **1986**, *19*, 267−272.

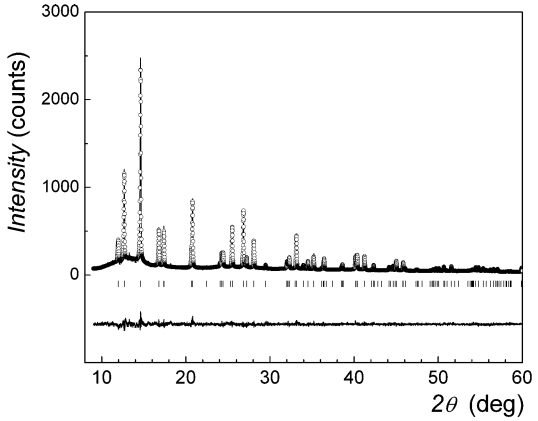

Figure 1. Final Rietveld refinement pattern of LaI. The calculated profile is denoted by "○"; the solid line corresponds to the observed pattern; vertical bars indicate the calculated reflection positions for LaI. The bottom trace represents the difference between the experimental and the calculated values.

$\rho_{calcd} = 6.80$ g/cm^3, absorption coefficient $\mu = 27.93$ mm^{-1}; number of reflections 102, number of variable parameters 10, $R_p = 0.0848$, $R_{wp} = 0.1110$, $R_{exp} = 0.1011$, $R_B = 0.0655$. Further details on the crystal structure refinement are listed in the Supporting Information.

Electronic Structure Calculations. First-principles density function theory band structure calculations for LaI were carried out in the local density approximation using the Stuttgart TB-LMTO-ASA program.[24] The eigenvalue problem was solved on the basis of the von Barth−Hedin local exchange-correlation potential[25] taking relativistic effects into account except for the spin−orbit coupling. The *k* space integration was performed using the tetrahedron method[26] to generate 793 irreducible points within the hexagonal Brillouin zone. Further computational parameters are given in Supporting Information. In addition, a topological analysis of the electron localization function (ELF)[27,28] as well as a study of the crystal orbital Hamiltonian population (COHP)[29] was performed to get a better insight into chemical bonding in LaI.

Physical Properties. Electrical resistance *R* was determined on pressed pellets of 3 mm diameter (thickness $h \sim 0.5$ mm) by the van der Pauw method[30] in a temperature range of 10−290 K. The samples were connected to gold wire contacts of a four-point probe setup using commercial silver paste (Epo-Tek H20E, Polytec, Germany). Each $R(T)$ curve was recorded both in cooling and in heating modes by measuring the voltage when a constant current of 1 mA was applied. To approximately evaluate the resistivity values we used the van der Pauw formula $\rho(\Omega\ \text{cm}) \approx R(\Omega)h(\text{cm})\pi/\ln 2$.

Magnetization measurements were performed with a SQUID magnetometer (MPMS, Quantum Design, 6325 Lusk Boulevard, San Diego) between 2 and 350 K in direct current magnetic fields $H = 1$, 3, and 5 T. A polycrystalline sample of about 30 mg was pressed into a pellet and sealed in a silica ampule under 1 atm He exchange gas to provide sufficient thermal contact. The magnetic data were corrected for the sample holder contribution and for the diamagnetism of the constituent atoms estimated from Pascal's increments (La^{3+}, -20×10^{-6} cm^3/mol; I^-, -52×10^{-6} cm^3/mol).[31]

Results and Discussion

LaI is synthesized by metallothermic reduction either of LaI_2 or of LaI_3 in a Na melt under argon at moderate temperatures (500−550 °C). The reaction between LaI_2 and Na was found to be sensitive to reaction times. Annealing of the reaction mixture at 550 °C for 3 days yields a mixture of LaI (≈ 20%), NaI, and LaI_2 (major phases), whereas the reaction is almost complete after 15 days. The finally isolated product contained a microcrystalline powder with a light golden appearance and a few black platelike LaI_2 crystals, which can be mechanically separated from the major phase. According to DTA of the LaI_2/Na samples, LaI is formed at 490−540 °C and melts incongruently in the range 690−740 °C. DTA measurements on several LaI_2/NaI mixtures indicate a composition independent endothermic effect at 470 °C which we associate with eutectic melting. The optimal reaction temperatures are thus between 550 and 680 °C.

The reaction between trihalide LaI_3 and sodium is complete within 3 days. However, it yields a mixture of NaI, LaI, and a fine La powder. The latter is hard to separate from the main product so that samples prepared by this route cannot be used for physical characterization. On the other hand, the formation of lanthanum metal through reaction of LaI_3 and Na implies a different reaction mechanism in the case of the metallothermic reduction of lanthanum trihalide and dihalide, respectively. The reaction with LaI_3 may be viewed as a sequence of two subreactions, namely, reduction of LaI_3 to metal and subsequent synproportionation. Another reaction mechanism is suggested for the metallothermic reduction of layered LaI_2, because no traces of La metal have been detected in the products prepared by this route. Here, it is worth pointing out that after extraction of NaI from the reaction products unreacted crystals of LaI_2 are changed in color from shiny violet to black and become delaminated into many layers (Figure 2), which are very easy to cleave when touched. Apparently, the alkali metal halide is formed within the layered LaI_2, which hints at an intermediate step of Na intercalation. In the present case the rate-limiting step appears to be the diffusion of sodium into LaI_2, resulting in slower reaction rates with respect to the reaction of LaI_3.

Figure 1 shows the X-ray powder diffraction pattern of a selected LaI sample used for further physical measurements. The sample is free of impurities and crystallizes in the hexagonal NiAs-like structure with lattice parameters $a = 3.9292(2)$ and $c = 9.712(1)$ Å, being in good agreement with those reported earlier.[5] The unusually large ratio of $c/a = 2.47$ found in LaI indicates stronger metal−metal interactions within the *ab* plane (3.93 Å) than along the *c* direction (4.85 Å). In this sense, LaI is in contrast with all known NiAs-type structures, for which the metal−metal interaction along *c* is prevalent.

The homogeneity and composition of the sample were checked by EDX analysis. Several analyses were carried out

(24) Tank, R. W.; Jepsen, O.; Burkhardt, A.; Andersen, O. K. *TB-LMTO-ASA 4.7*; Max-Planck Institut für Festkörperforschung: Stuttgart, Germany, 1998.
(25) Von Barth, U.; Hedin, L. *J. Phys. C* **1972**, *5*, 1629−1642.
(26) Blöchl, P. E.; Jepsen, O.; Andersen, O. K. *Phys. Rev. B* **1994**, *49*, 16223.
(27) Savin, A.; Becke, A. D.; Flad, J.; Nesper, R.; Preuss, H.; von Schnering, H. G. *Angew. Chem.* **1991**, *103*, 421−424; *Angew. Chem. Int. Ed. Engl.* **1991**, *30*, 409−412.
(28) Silvi, B.; Savin, A. *Nature* **1994**, *371*, 683−686.
(29) Dronskowski, R.; Blöchl, P. E. *J. Phys. Chem.* **1993**, *97*, 8617−8624.
(30) Van der Pauw, L. J. *Philips Res. Rep.* **1958**, *13*, 1−9.
(31) Carlin, R. L. *Magnetochemistry*; Springer Publishers: Berlin, 1986.

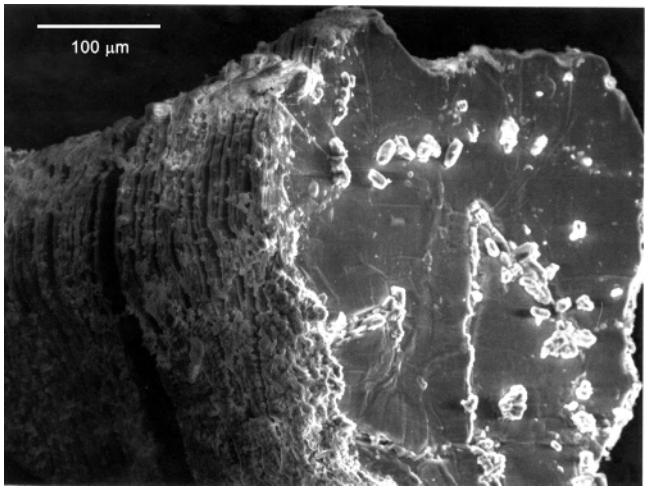

Figure 2. Micrograph of a LaI_2 crystal after treatment of the reaction products (NaI/LaI/LaI_2) with diglyme.

on different crystals, all of them showing a ratio of La/I close to 1. The mean value of the eleven-point analyses results in $La_{1.01(1)}I_{0.99(1)}$. Line scans and spectral imaging within one crystal indicate no variations of the La/I ratio; however, traces of oxygen were detected. The relative amount of oxygen depends on the thickness of the transmitted area; that is, it becomes more significant in very thin areas, particularly in amorphous surface layers. There are no indications that the oxygen is an intrinsic part of the crystal structure of LaI.

The metrics of the crystallites was analyzed by SAED. All measured *d* values are consistent with the ones expected for a NiAs-type structure of LaI, for example, $d(100)_{exp}$ = 3.4 Å (calcd, 3.40 Å) and $d(001)_{exp}$ = 9.7 Å (calcd, 9.71 Å). Tilting experiments gave additional support to the assignment of the NiAs-type metrics. Starting from the [001] zone axis, a tilt of about 21.5° (lit., 22°) along the direction ⟨100⟩* allows several zone axes of the type ⟨011⟩ to be adjusted. No significant deviations in the intensity distribution of the ⟨011⟩ patterns occur, thus confirming that the zone axes ⟨011⟩ are symmetry equivalent.

The intensity in the experimental SAED patterns is affected by multiple diffraction and strongly depends on the thickness of the transmitted area. Therefore, we observed characteristic deviations of the intensity distribution of experimental and simulated patterns based on the kinematical approximation, cf. Figure 3. Those deviations concern all reflections, even the kinematically forbidden ones. The simulation of the dynamical intensity in dependence of the specimen's thickness proves the strong excitation of kinematically weak reflections, for example, $00\bar{2}$ (see Figure 3). The influence of multiple scattering on kinematically forbidden reflections was checked by tilting experiments. In the zone axis [100] strong violations of the serial reflection condition 00*l* with *l* = 2*n* (space group $P6_3/mmc$) were observed. The influence of multiple diffraction effects can be reduced by tilting from the precise zone axis orientation around [001]*. The intensity of 00*l* with *l* = 2*n* is not affected by the tilt, while the kinematically forbidden reflections vanish completely after

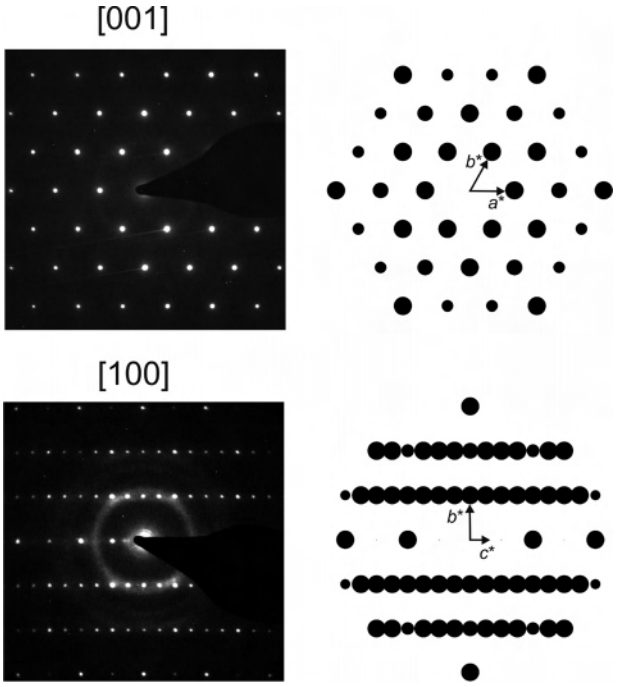

Figure 3. Experimental (left) and calculated (right) SAED patterns of LaI along different zone axes.

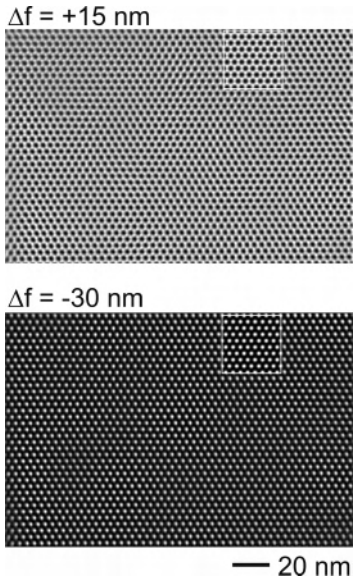

Figure 4. HRTEM micrographs along [001]. Shown in the insets are image simulations (crystal thickness, 9.7 nm; defocus values specified in the image).

applying a tilt of 15°. Hence, a symmetry reduction as the source of the violations of the reflection conditions can be excluded.

All crystals are characterized by a perfect three-dimensional structure; that is, no domains, stacking faults, or other kinds of crystal defects can be detected by HRTEM. As evidenced by the Fourier transformation all HRTEM micrographs along [001] display a perfect hexagonal symmetry 6*mm*. The micrographs of Figure 4 were recorded in the same area of one crystallite with different defocus values. The black and white contrasts do not correspond with the projected potential; hence, a direct correlation to a projection of the structure is not feasible. However, the good agreement

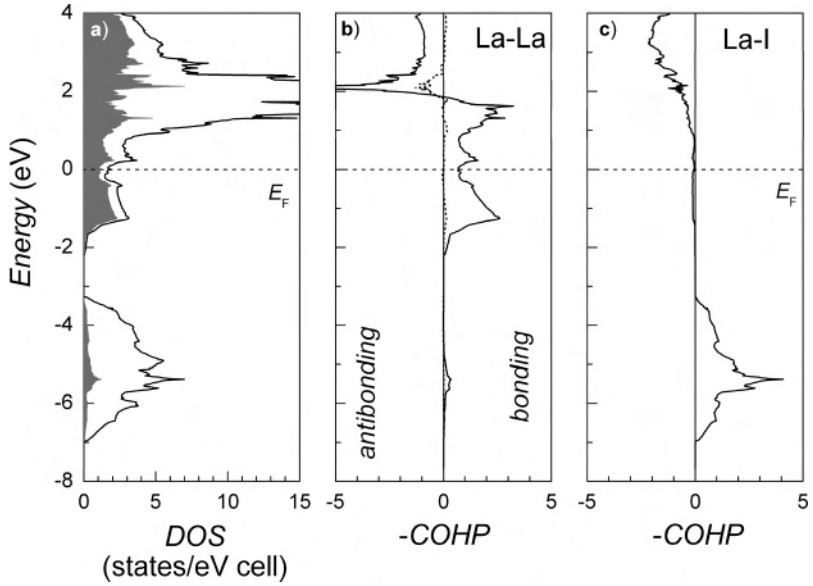

Figure 5. (a) Electronic DOS for LaI with partial contributions of lanthanum 5d states (filled area). The dashed line displays the position of the Fermi level. (b) COHP diagram of the La−La bonds in LaI. The dotted line represents the contribution of the interlayer La−La interactions (4.85 Å) along the *c* axis. (c) COHP diagram of the La−I bonds in LaI.

to the inserted simulated images again demonstrates that the structure of LaI corresponds with the NiAs-type structure anticipated for the simulations. To conclude, all electron microscopy observations are consistent with the established composition and structure of LaI.

According to semiempirical Extended Hückel band structure calculations,[5] LaI is expected to exhibit metallic yet strongly anisotropic transport properties. To get deeper insight into the electronic structure and chemical bonding, the densities of states (DOS), ELF (η), and selected COHP have been calculated with the first principles LMTO method. Figure 5a presents the electronic DOS for LaI. The bonding combinations of the I 5p states together with the 5s and 5p states of lanthanum form the valence band manifold between −7 and −3 eV relative to the Fermi level, E_F. The area at $E > -2$ eV is mainly comprised of the La 5d and 4f states (above E_F) with the predominant contribution of the d_{xy} and d_{z^2} orbitals in the vicinity of E_F. The Fermi level crosses the conduction band between two high-density regions resulting in a DOS at the Fermi level of $N(E_F) \cong 1.0$ states eV^{-1} per formula unit.

The ELF consists of nearly spherical localization domains ($\eta^{max} = 0.73$) around the iodine ions and bonding attractors ($\eta^{max} = 0.56$) that are localized in the center of the metal atom triangles. The topology of the latter can easily be attributed to three-center (3c) bonds. It is interesting that the bonding attractors do not lie exactly within the metal atom plane but are slightly shifted along the *c* axis in a way to minimize electronic repulsion between bonding orbitals and capped iodine ions (see Figure 6). The 3c attractor basins merge at $\eta = 0.56$ so that a channel-like honeycomb network structure of interconnected domains is visualized in the representation shown in Figure 6. The electronic count for LaI can thus be formulated as $(La^{3+})(I^-)\cdot 2e$, where two extra electrons are involved in La−La bonding. However, the metal−metal bonding is unsaturated because there are four

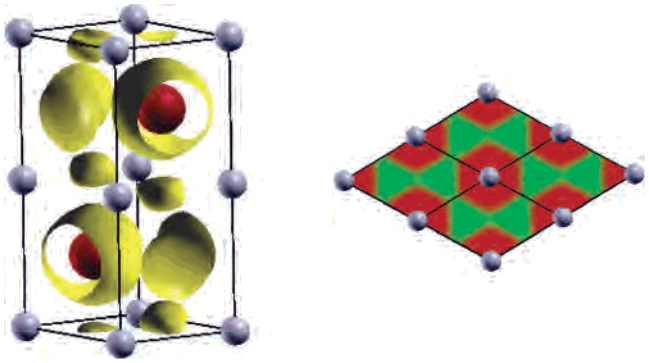

Figure 6. ELF (η) in the LaI structure (grey spheres La, red spheres I). Left: ELF isosurface with $\eta = 0.32$ showing the bonding attractors for La−La bonds and "core" attractors for I ions. Right: ELF representation as a contour slice through the (001) plane of the hexagonal unit cell (red, $\eta < 0.1$; green, $\eta \approx 0.4$).

bonding "3c−2e" attractors per unit cell sharing four valence electrons. This conclusion is further supported by the COHP analysis of M−M interactions. Figure 5b displays the COHP curve of the La−La bonds in LaI. The bonding states are not completely filled up to the Fermi level E_F, indicating that the electron count is far from that of optimized La−La bonding. On the other hand, the Fermi level is adjusted in such a way to avoid the occupation of strongly antibonding La−I states (see Figure 5c). For comparison of bond strengths we have analyzed integrated COHP values (ICOHP) of the intralayer and the interlayer La−La interactions. The shorter in-plane La−La distances of 3.93 Å have an ICOHP value of −0.46 eV/bond, compared with one of −0.07 eV/bond for the longer interlayer La−La distances of 4.86 Å. This relation indicates a much weaker, if any, interaction between the metal atoms along the *c* axis.

In agreement with the band structure calculations, LaI exhibits typical metallic behavior with decreasing electrical resistance toward low temperature (Figure 7). The absolute values ρ are rather high for a metallic material and seem to

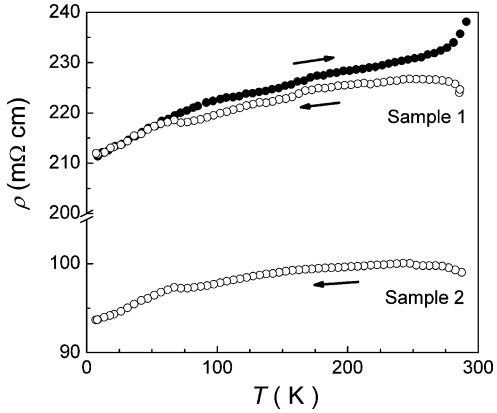

Figure 7. Temperature dependences of the electrical resistivity ρ for two different LaI samples, measured both in cooling and heating modes. For clarity, $\rho(T)$ data for the sample 2 are shown only as a function of decreasing temperature.

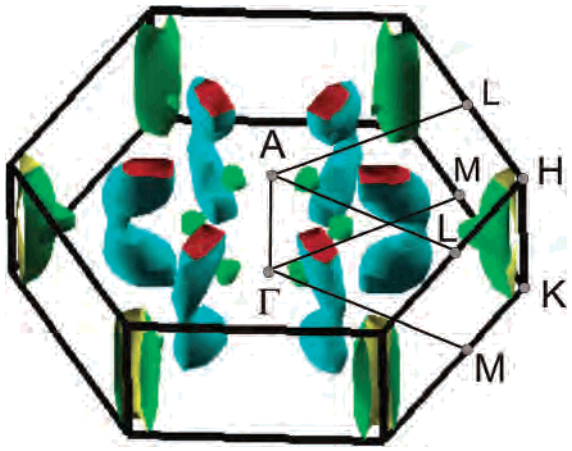

Figure 8. Fermi surface of LaI. The first Brillouin zone with characteristic high-symmetry points [$\Gamma = (0,0,0)$, $K = (2\pi/3a,2\pi/3a,0)$, $M = (\pi/a,0,0)$, $A = (0,0,\pi/c)$, $H = (2\pi/3a,2\pi/3a,\pi/c)$, and $L = (\pi/a,0,\pi/c)$] is outlined.

be unreliable because those measured on two different pellets from the same sample batch differ by a factor of about 2. This is likely due to the grain boundary and surface effects as the latter may be contaminated by traces of insulating NaI and/or diglyme molecules. However, a remarkable and reproducible feature is a small maximum in the resistivity at $T_{max} = 67$ K, seen only in the cooling mode. This anomaly disappears upon heating a sample, yielding a hysteresis in $\rho(T)$ above 70 K. It is interesting that the resistance anomaly observed resembles features, which are observed in layered transition metal dichalcogenides and bronzes with nested Fermi surfaces and associated with charge density waves (CDW) formation.[32,33] Such compounds have a tendency to lower their electronic energy by undergoing a lattice distortion, causing characteristic anomalies in the electrical and magnetic properties due to induced modulation of the electronic density at the Fermi level (CDW instability). It is interesting that nesting motifs are also found in the calculated Fermi surface of LaI (see Figure 8). It consists of two parts: two concentric hole cylinders centered at K and six anisotropic electron cylinders oriented along the c^* direction, which are located between the Γ and K points and are capped with electron pockets at $c^*/2$ and c^*, respectively. The cylindrical electron Fermi surfaces are squeezed along the $[\bar{1}20]^*$ direction, providing nesting regions with a nesting vector parallel to this direction. However, the nesting is much weaker than in the case of layered transition metal compounds.

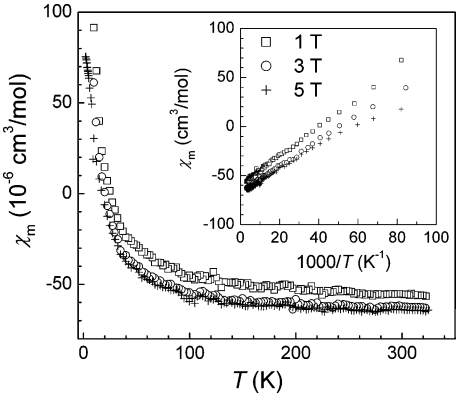

Figure 9. Temperature dependences of the magnetic susceptibility χ_m for LaI, measured at various magnetic fields. The inset shows χ_m as a function of inverse temperature. Extrapolated values ($1/T \rightarrow 0$) correspond to the temperature independent contribution χ_0.

Magnetic measurements reveal no anomaly in the magnetic susceptibility of LaI around T_{max}. The sample shows weak temperature dependent paramagnetic behavior (Figure 9), which we attribute to a small contamination of the sample by magnetic impurities, likely to originate from the starting La metal pieces.[34] The susceptibility data can be fitted to a modified Curie law, $\chi_m = C/T + \chi_0$, where the Curie term C/T accounts for the paramagnetic impurities, and the temperature independent part, χ_0, includes the diamagnetic contribution χ_{dia} from the closed electronic shells and the Pauli paramagnetic component χ_{Pauli} from the conduction electrons. The Curie constant C derived from the fits corresponds to approximately 300 ppm of $S = 7/2$ entities (e.g., Gd^{3+} ions) per formula unit. The extrapolation of the data $1/T \rightarrow 0$ directly provides $\chi_0 = -65(5) \times 10^{-6}$ cm^3/mol. After subtracting the core diamagnetism ($\chi_{dia} = -72 \times 10^{-6}$ cm^3/mol), the Pauli susceptibility of $\chi_{Pauli} \approx 10^{-5}$ cm^3/mol is obtained for LaI, which is an order of magnitude smaller than that reported earlier.[5] The observed χ_{Pauli} is in turn approximately three times smaller than the value of 32×10^{-6} cm^3/mol, estimated from the band structure calculations according to $(\chi_{Pauli})_{calcd} = N(E_F)\mu_B^2$.[35] More detailed studies on single crystals of LaI will be necessary to understand the physical properties of this compound with a strongly anisotropic electronic structure more quantitatively.

Conclusion

LaI can be synthesized by metallothermic reduction of LaI_2 with sodium in welded Ta ampules filled with argon. The

(32) Wilson, J. A.; Di Salvo, F. J.; Mahajan, S. *Adv. Phys.* **1975**, *24*, 117.
(33) Schlenker, C.; Dumas, J.; Escribe-Filippini, C.; Guyot, H. In *Low dimensional properties of molybdenum bronzes and oxides*; Schlenker, C., Ed.; Kluwer Academic Publishers: Dordrecht, 1989.
(34) Ryazanov, M.; Simon, A.; Mattausch, Hj.; Kremer, R. K. *J. Alloys Compd.* **2004**, *374*, 142−145.
(35) Ashcroft, N. W.; Mermin, N. D. *Solid State Physics*; Saunders College Publishing: Philadelphia, 1976.

main advantage of this method with respect to a synproportionation reaction of LaI_3 and La consists of a decrease of the reaction temperature as well as of a considerable reduction of the reaction time, whereby LaI can be obtained in high yields, opening new prospects for further investigations. However, LaI needs to be separated from NaI formed during the reaction as well as from unreacted LaI_2 crystals. The topological analysis of the ELF and calculations of the COHPs indicate three-center bonding between the metal atoms within the *ab* plane and almost no covalent interaction along the *c* direction. This is quite unusual for the NiAs-type structures, for which bonding M−M interactions along the *c* axis are a characteristic feature. Electrical resistivity and magnetization measurements confirm the metallic behavior for LaI in accordance with the electronic structure calculations. Nonetheless, the DOS value at the Fermi level estimated from the Pauli magnetism is three times smaller than that obtained from the LMTO calculations.

Acknowledgment. We gratefully thank G. Siegle for the electrical resistivity measurements, E. Brücher for the magnetic measurements, and V. Duppel for the expert assistance in HRTEM and EDX experiments.

Supporting Information Available: Tables of crystallographic and refinement parameters and parameters of the TB-LMTO-ASA calculations, as well as LMTO band structure of LaI in the fat band representation showing contributions of selected La (5s, 5p, and 5d) atomic orbitals. This material is available free of charge via the Internet at http://pubs.acs.org.

IC051834R